# Non-Coherent Detection for Ultraviolet Communications with Inter-Symbol Interference

Wenxiu Hu, Zhuangkun Wei, Sergei Popov, *Member, IEEE, Fellow, OSA,* Mark Leeson, *Senior Member, IEEE,* Min Zhang, Tianhua Xu *Member, IEEE*

***Abstract*—Ultraviolet communication (UVC) serves as a promising supplement to share the responsibility for the overloads in conventional wireless communication systems. One difficulty lies in how to address the inter-symbol-interference (ISI) from the strong scattering nature and the time-varying channel response. This is more challenging for the energy-constrained scenarios (e.g., underwater UV), as existing coherent schemes (i.e., requiring exact channel information for signal detection) become less attractive given the computational and storaging complexity for repeated time-varying channel estimation and statistical signal detection. In this work, a novel non-coherent paradigm is proposed, via the exploration of the UV signal features that are insensitive to the ISI. By optimally weighting and combining the extracted features to minimize the bit error rate (BER), the optimally-weighted non-coherent detection (OWNCD) is proposed, which converts the signal detection with ISI into a binary detection framework, with a heuristic weight updating approach for time-varying channel. As such, the proposed OWNCD avoids the complex channel estimation and guarantees the detection accuracy. Compared to the state-of-the-art coherent maximum likelihood sequence detection (MLSD) in the cases of static and time-varying channel response, the proposed OWNCD can gain $\sim$1 dB and $\sim$8 dB in signal-to-noise-ratio (SNR) at the 7$\%$ overhead forward-error-correction (FEC) limit (BER of $4.5 \times 10^{-3}$), respectively, and can also reduce the computational complexity by 4 order of magnitude.**

***Index Terms*—Ultraviolet communications, inter-symbol interference, time-varying channel, non-coherent detection.**

## I. Introduction

Ultraviolet communication (UVC) has been regarded as a promising supplement for conventional wireless communication systems, due to its strong scattering induced non-line-of-sight (NLoS) [1], [2] and the solar-blind property [1]–[5]. This has led to significant research efforts, ranging from the development of UVC devices [6]–[9], model formulations [2], [10]–[14], design of channel coding schemes [15]–[18], to detection scheme design [19]–[23].

Compared with other wavelength free space optics (FSOs) that require strict alignment for transceivers, the NLoS characteristic enables the flexible deployment of UVC systems, thereby widening its potential applications in some adverse communication environments. These include underwater communications [24], multi-hop networks [1], and military/battlefield applications [25]; all of these have the following two challenges that cause communication performance deterioration. First, the stronger UV photon scattering nature, compared with other wavelength FSOs, gives rise to more intensive inter-symbol-interference (ISI) [1], [20], [22]. Second, applications in adverse communication environments (e.g., underwater, and battlefield) combined with the flexible device deployment may produce a time-varying channel effect. This will be even worse in the case of energy and resource constrained scenarios (e.g. underwater, where re-charging a device is difficult), which make the complex statistical and sequential detection schemes less attractive.

The first challenge has been well studied by most of the coherent detection schemes in [20]–[23], which leverage on the estimation of the channel impulse response (CIR) to infer the channel state information (CSI) for ISI compensation and signal detection. The state-of-the-art maximum likelihood sequence detection (MLSD) employed in [20], using a pilot sequence for least square (LS) CIR estimation and maximizing the likelihoods for signal detection, performs well in generic linear time-invariant FSO modelling. However, the scheme is less attractive when addressing the signal detection in the time-varying UV channel, especially for energy-constrained scenarios, as it will fall into either repeated channel estimation requiring long pilot sequence overheads and substantial computational complexity, or poor CSI acquisition that further hinders the detection performance.

In contrast to coherent detection, non-coherent detection focuses on extracting the useful features from the inherent characteristics of the received signals, rather than resorting to the CSI estimation and statistical inference that have higher computational complexity [26]. The popular non-coherent schemes for negligible ISI scenarios are listed in [19], [27]–[29], which unfortunately will saturate to a bit error rate (BER) floor [19], [27] in the context of UVC that has intensive ISI. To address the ISI challenge, a novel non-coherent scheme in [30] has been proposed for molecular communications. By extracting the transient features of the molecular signal, such a non-coherent scheme can combat the ISI inherently rather than via complex steps of channel estimations. However, the non-coherent scheme for molecular communications 1) cannot adjust to the time-varying channel occuring in UVC, and 2) overlooked some important UV signal-features given

This work is supported in part by UK EPSRC Program Grant TRANSNET (EP/R035342/1) and in part by EU Horizon 2020 RISE Grant (No. 778305). M. Zhang is supported by National Natural Science Foundation of China (NSFC 61975020). ($Corresponding\ author:\ Tianhua\ Xu$). W. Hu, Z. Wei, M. Leeson and T. Xu are with School of Engineering, University of Warwick, Coventry CV4 7AL, UK. T. Xu is also with Tianjin University, Tianjin 300072, China and University College London, London WC1E 6BT UK (tianhua.xu@ieee.org). S. Popov is with Department of Applied Physics, KTH Royal Institute of Technology, Sweden (sergeip@kth.se). M. Zhang is with Institute of Information Photonics and Optical Communications, Beijing University of Posts and Telecommunication, Beijing 100876, China (mzhang@bupt.edu.cn).

the different levels of particulate nature between molecules and UV photons (we provide the performance in Figs. 4-6). As such, these challenges constitute the motivation to design a novel non-coherent scheme that can counteract the ISI contamination for UVCs.

In this paper, to address the aforementioned two challenges, we propose a novel non-coherent detection scheme, leveraged on the linearly weighted combinations of the transient features of the UV signal. To sum up, the main contributions are listed as follows.

(1) We extract four features of optical signals, which reflect the intra-symbol rising edge, the intra-symbol energy, the inter-symbol minimum inflexion, and the inter-symbol energy difference of the signal respectively. The key advantage of such features lies in their abilities to inherently counteract the ISI without the complex channel estimation process adopted by coherent detection schemes, since the extracted features are insensitive to the ISI contamination (see Fig. 2).

(2) Leveraged on the extracted four features, we optimally weight and combine such features, and propose a novel non-coherent scheme called optimally-weighted non-coherent detection (OWNCD). The closed-form formulas of the optimal weights are computed via the minimization of the theoretical BER. As such, the proposed OWNCD is able to convert the detection scenarios with ISI into a binary detection framework, which avoids the complex channel estimation process that aims to construct the CSI for ISI compensation. Also, compared with the previous non-coherent scheme in [30], the proposed OWNCD is able to adjust the optimal weights with respect to the different levels of the ISI intensities, and therefore delivers a better detection performance.

(3) For the time-varying channel response, we further design a heuristic algorithm to adaptively achieve the optimal weights. Such a heuristic algorithm relies on the previous data that can reflect the continuous changes in the channel environment, thereby capable of addressing the time-varying UV channel challenges (which is demonstrated in Fig. 5). Also, by utilizing only addition and multiplication operations, the heuristic implementation renders a lower complexity advantage as opposed to the coherent MLSD in [20], in which complex exponential and logarithm operations are necessary to build the likelihood probability.

(4) The detection performance of the proposed OWNCD scheme is numerically evaluated. Compared to the state-of-the-art coherent MLSD in the cases of static and time-varying CSI, the proposed OWNCD can gain $\sim$1 dB and $\sim$8 dB in signal-to-noise-ratio (SNR) at the $7\%$ overhead forward-error-correction (FEC) limit (BER of $4.5 \times 10^{-3}$), respectively, and has also reduced the computational complexity by four orders of magnitude. Meanwhile, the OWNCD outperforms the conventional non-coherent scheme in [30] by nearly 4 dB in SNR. As such, our proposed feature-based OWNCD technique provides a promising pathway for the efficient detection in complex and dynamic wireless optical channels with intensive ISI caused by photon scattering.

The rest of the paper is structured as follows. In Section II, the underlying UVC model is described, along with the problem formulation. In Section III, we elaborate our proposed optimal weighted non-coherent detection scheme. The numerical simulation is provided in Section IV. We finally conclude the work in Section V.

## II. System models and Problem Formulation

### A. UVC System

A generic UVC system is shown in Fig. 1, which consists of a UV transmitter, a UV channel, and a UV receiver.

*1) UV transmitting module:* The UV transmitting module aims at modulating and transmitting the input information into the UV channel. See Fig. 1. In this work, the input information is the binary signal string, which will be modulated by an on-off keying (OOK) modulator and then the LED transmitter. By denoting the binary information by $s_k = j \in \{0, 1\}$ $(k = 1, \cdots, +\infty)$, the transmitted UV signal in terms of the number of photons, $s(t)$ is expressed as:

$$s(t) = \sum_{k=1}^{\infty} s_k \cdot \delta\left(t - kT_b\right) \otimes \omega(t), \tag{1}$$

where $T_b$ is the symbol interval, $\otimes$ denotes the convolution operator, and $\omega(t)$ is the pulse shape of the UV-LED transmitter. Here, we adopt a rectangular pulse, i.e., $\omega(t) = N_T/T_p \cdot rect((t - T_p/2)/T_p)$, with $N_T$ the transmitted number of UV photons for single '1'-bit, and $T_p$ the pulse width.

*2) UV channel:* The UV CIR, denoted by $h(t)$, is governed by the transmission distance (i.e., $r$), the transmitter's beam divergence $\theta_T$ and apex angle $\beta_T$, the receiver's half-field of view $\theta_R$ and apex angle $\beta_R$, and the atmospheric based channel parameters [20], [22]. Differing from other FSOs that are limited by strict device alignment, in NLoS enabled UVC that allows flexible configuration, such channel parameters can have small perturbations (noise), which makes the UV channel time-varying and difficult for traditional channel estimation technologies. In this work, our design of non-coherent scheme does **not** require the exact CIR formulas, but only the transient shapes that are insensitive to time-varying $h(t)$ induced by random parameter perturbations. For the simulation part, we use the Monte-Carlo process in [10], [11] to obtain the CIRs $h(t)$ that result from different channel parameters.

An illustration of two CIRs is provided in Fig. 1. Note that although the exact shapes of the CIRs may change drastically with their channel parameters, the transient features of such CIRs are in common (e.g., an obvious rising edge for the appearance of an 1-bit). These give an inspiration for designing the non-coherent detection scheme in the receiver, by exploiting such features of the UV signal.

*3) UV receiver:* As is shown in Fig. 1, the receiving process begins at the photo detector (e.g., photomultiplier tube, PMT [1]), which converts the received UV signal by photoelectric-conversion. Then, the oscilloscope derives samples of the converted electrical signal for further non-coherent signal detection unit processing.

Given the study in [20], by assigning the sampling rate of oscilloscope as $T_s = T_b/M$, the number of received UV pho-

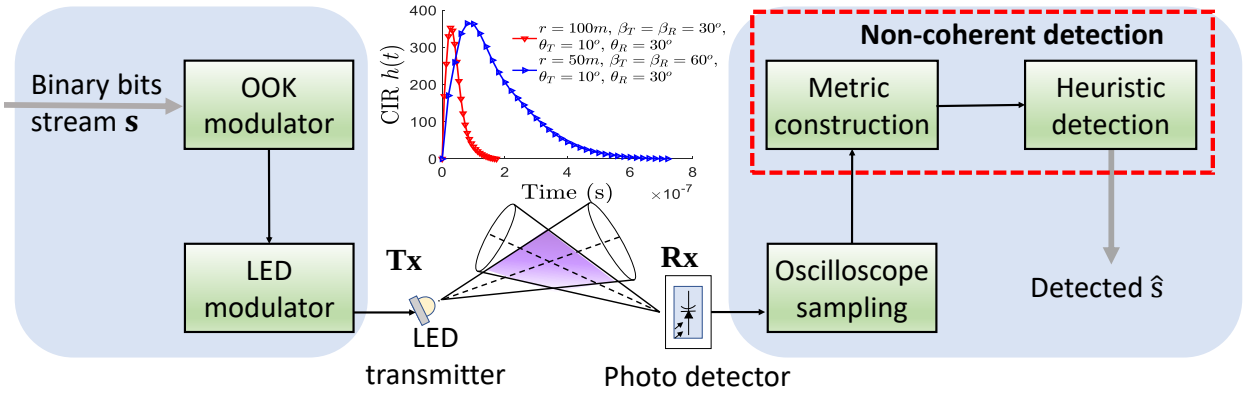


Fig. 1. Illustration of UVC system with a LED-transmitter, UV channel, and a UV photon-counting receiver. The non-coherent detection scheme is deployed at the end of the receiver, whereby metrics are constructed at first, followed by the Heuristic detection.

tons within time $((i-1)T_s, iT_s], i \in \{(k-1)M+1, \cdots, kM\}$, denoted as $n_i$, follows the Poisson distribution, i.e., [20]

$$n_i \sim \mathcal{P}\left(\sum_{l=k-L+1}^{k} \bar{n}_{i-(l-1)M} \cdot s_l + \bar{\epsilon}\right). \tag{2}$$

In Eq. (2), $\mathcal{P}(\cdot)$ denotes the Poisson distribution; $L$ is the length of ISI, indicating the influence of the previous $L$ symbols on the currently received signal; $\bar{\epsilon}$ is the expectation of the number of received background noise photons; $\bar{n}_{i-(l-1)M}$ is the mean of received number of UV photons emitted at at $l$th symbol interval, i.e., [20]

$$\bar{n}_{i-(l-1)M} = \int_{(i-(l-1)M-1)T_s}^{(i-(l-1)M)T_s} h(t) \otimes \omega(t) dt. \tag{3}$$

Furthermore, after the photoelectric-conversion, the discrete electric signal at sampling time $iT_s$ is:

$$\begin{aligned} y_i &= \alpha \cdot n_i + \varepsilon_i \\ &= \underbrace{\alpha \bar{n}_{i-(k-1)M} \cdot s_k}_{\text{current signal}} + \underbrace{\alpha \sum_{l=k-L+1}^{k-1} \bar{n}_{i-(l-1)M} \cdot s_l}_{\text{ISI}} + \underbrace{\varepsilon_i}_{\text{noise}}, \end{aligned} \tag{4}$$

where $\alpha = A \cdot h \cdot \nu$ with $A$ the photoelectric-conversion parameter, $h = 6.626 \times 10^{-34}$Js the Plunk constant, and $\nu = 3.77 \times 10^6$GHz the frequency of UV beam. Here, $\varepsilon_i \sim \mathcal{N}(\mu, \varsigma^2)$ represents the noise of device, and is assumed to follow Gaussian distribution whose variance is dominated, i.e., $\varsigma^2 \gg \bar{\epsilon} + \sum_{l=k-L+1}^{k} \bar{n}_{i-(l-1)M} \cdot s_l$), given the negligible in-band counting noise due to solar-blind property of UVC.

### B. Problem Formulation

Given the expressions of the received signals in Eq. (4), the purpose of this work is to detect the current information bit $s_k$ from the received signal $\mathbf{y}_{1:kM} = [y_1, ..., y_{kM}]^T$. Here, it is noteworthy that the exact form of the CIR $h(t)$, and the variance of the noise $\varepsilon_i$ are unavailable, varying with the changes of the channel parameters and the uncertainties of the Rx, and the PMT detector.

It is noteworthy that coherent detection schemes (e.g., MLSD in [20]) are not suitable for UVC with its time-varying channel response and resource constraints, as they will lead to (i) the heavy pilot overheads to track the changes of the CIR, and (ii) computational and storage complexity for the computation of posterior (or likelihood) probability. This makes the design of a non-coherent scheme necessary, which will be elaborated in the following sections.

## III. Optimal Weighted Non-coherent Detection

In this section, we elaborate our proposed non-coherent detection scheme. By exploiting the transient features of the optical signals, the decision metric is directly derived from the observations $y_i$ for signal detection, which completely excludes the complex CSI estimations.

### A. Optical Feature Extraction

We firstly extract four features via the exploration of the intra-symbol rising edge, the intra-symbol energy, the inter-symbol minimum inflexion, and the inter-symbol energy difference. We then list the advantages of such extracted features.

*1) Intra-symbol rising-edge:* Taking the $k$th interval with $M = T_b/T_s$ samples as an example, in the case of $s_k = 1$, the output $y_i$ will produce a distinct rising edge. Otherwise, when $s_k = 0$, $y_i$ shows a slow decay. As shown in Fig. 2(a), this rising edge can be expressed by the difference of its maximum (computed by averaging its neighbourhood $\mathcal{R}_{\max}$) from the initially $\mathcal{R}_0$, i.e.,

$$z_{k,1} \triangleq \sum_{i \in \mathcal{R}_{\max}} y_i - \sum_{i \in \mathcal{R}_0} y_i. \tag{5}$$

where $|\cdot|$ denotes the width (number of elements) of a set, and we assign the widths of $\mathcal{R}_{\max}$ and $\mathcal{R}_0$ to be $|\mathcal{R}_{\max}| = |\mathcal{R}_0| = M/4$

The distribution of $z_{k,1}$ is analyzed as follows. Given Eq. (5), $z_{k,1}$ is the linear summation of the independent observations $y_i$, whose distribution is Gaussian according to Eq. (4). As such, the probabilistic distribution of $z_{k,1}$ can be

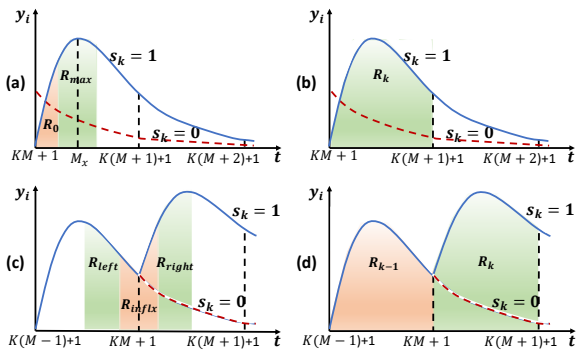


Fig. 2. Illustrations of four features, where (a) gives the intra-symbol rising-edge, (b) is the intra-symbol energy, (c) illustrates the inter-symbol minimum inflexion, and (d) provides the inter-symbol energy difference.

regarded as a Gaussian distribution, given the central limit theorem (CLT), i.e.,

$$z_{k,1}|s_k \sim \begin{cases} \mathcal{N}\left(\mu_{1,0},\ \sigma_1^2\right) & s_k = 0, \\ \mathcal{N}\left(\mu_{1,1},\ \sigma_1^2\right) & s_k = 1, \end{cases} \tag{6}$$

where $\mu_{1,0}$ and $\mu_{1,1}$ are the expectations for cases $s_k = 0$ and $s_k = 1$ respectively, and $\sigma_1^2$ is the variance of metric $z_{k,1}$.

*2) Intra-symbol energy:* Intra-symbol energy refers to the summation of samples in the current $k$th slot signal. This feature, overlooked by the previous study of a non-coherent scheme for molecular communications in [30], cannot be ignored in the context of UVCs. This is because the UV-beam exhibits less of a particulate nature than molecules, which suggests a shorter averaging suspended period for each particle (i.e., UV photon), and thereby a reduced intensity of ISI. As such, given the smaller ISI effect in UVCs, the intra-symbol energy is to some extent able to distinguish the difference between $s_k = 1$ and $s_k = 0$. As is shown in Fig. 2(b), we define the intra-symbol energy as:

$$z_{k,2} = \sum_{i \in \mathcal{R}_k} y_i, \tag{7}$$

with $\mathcal{R}_k = \{kM + 1, \cdots, k(M + 1)\}$.

Similar to the distribution of $z_{k,1}$, the distribution of $z_{k,2}$ is also Gaussian, and can be expressed as:

$$z_{k,2}|s_k \sim \begin{cases} \mathcal{N}\left(\mu_{2,0},\ \sigma_2^2\right) & s_k = 0, \\ \mathcal{N}\left(\mu_{2,1},\ \sigma_2^2\right) & s_k = 1, \end{cases} \tag{8}$$

where $\mu_{2,0}$ and $\mu_{2,1}$ are the expectations for cases $s_k = 0$ and $s_k = 1$ respectively, and $\sigma_2^2$ is the variance of metric $z_{k,2}$.

*3) Two Inter-symbol Properties:* We then analyze the transient features between two adjacent symbols. For two successive symbols in the slots $k - 1$ and $k$, we can notice from Fig. 2(c)-(d) that (i) the transient shape at the beginning of the $k$th symbol is distinguishable between $s_k = 1$ and $s_k = 0$, and (ii) there exists an obvious successive energy difference. As such, we adopt the previous designed sub-metrics (i.e., the inter-symbol minimum inflexion, and the inter-symbol energy difference), which are given as follows [30]:

$$z_{k,3} \triangleq -\sum_{i \in \mathcal{R}_{\text{inflx}}} y_i + \frac{1}{2}\left(\sum_{i \in \mathcal{R}_{\text{left}}} y_i + \sum_{i \in \mathcal{R}_{\text{right}}} y_i\right), \tag{9}$$

$$z_{k,4} \triangleq \sum_{i \in \mathcal{R}_k} y_i - \sum_{i \in \mathcal{R}_{k-1}} y_i, \tag{10}$$

where the widths are assigned as $|\mathcal{R}_{\text{inflx}}| = |\mathcal{R}_{\text{left}}| = |\mathcal{R}_{\text{right}}| = M/4$. Then, we give the distributions of $z_{k,3}$ and $z_{k,4}$ given the CLT, i.e.,

$$z_{k,3}|s_k \sim \begin{cases} \mathcal{N}\left(\mu_{3,0},\ \sigma_3^2\right) & s_k = 0, \\ \mathcal{N}\left(\mu_{3,1},\ \sigma_3^2\right) & s_k = 1, \end{cases} \tag{11}$$

$$z_{k,4}|s_k \sim \begin{cases} \mathcal{N}\left(\mu_{4,0},\ \sigma_4^2\right) & s_k = 0, \\ \mathcal{N}\left(\mu_{4,1},\ \sigma_4^2\right) & s_k = 1. \end{cases} \tag{12}$$

In Eq. (11), $\mu_{3,0}$ and $\mu_{3,1}$ are the expectations for cases $s_k = 0$ and $s_k = 1$ respectively, and $\sigma_3^2$ is the variance of metric $z_{k,3}$. In Eq. (12), $\mu_{4,0}$ and $\mu_{4,1}$ are the expectations for cases $s_k = 0$ and $s_k = 1$, and $\sigma_4^2$ are the variance of $z_{k,4}$.

*4) Advantages of Features:* The derived features in Eqs. (5)-(10) have three advantages.

First, each one transforms the observation $y_i$ that is heavily contaminated by ISI into a new domain that is insensitive to ISI. For instance, given a fixed intensity of the ISI and any of $s_k$, the expectations of $z_{k,1}$ $z_{k,2}$, $z_{k,3}$ and $z_{k,4}$ remain quasi-constant, as they reflect only the common features of the signal shapes. This suggests the inherent ability of the four features to counteract the ISI, without any process of complex channel estimations for ISI mitigation (as the coherent schemes do). As such, the extracted features convert the detection with ISI into a binary detection framework, enabling the potential designs of the non-coherent schemes.

Second, the utilisation of the neighbouring sets i.e., $\mathcal{R}_{\text{max}}$, $\mathcal{R}_0$, $\mathcal{R}_{\text{inflx}}$, $\mathcal{R}_{\text{left}}$, $\mathcal{R}_{\text{right}}$ and $\mathcal{R}_k$ avoids the sensitivity to channel parameter perturbation induced time-varying channel response. Such neighbourhoods of which the expectations of the elements changes smoothly helps neutralize the noise effects by the mechanism of averaging filters.

Third, the four features $z_{k,1}$ $z_{k,2}$, $z_{k,3}$, and $z_{k,4}$ share the same positiveness and negativeness for the case $s_k = 1$ and $s_k = 0$ respectively. That is, $\mu_{1,0}$ $\mu_{2,0}$ and $\mu_{3,0}$ are all negative and $\mu_{1,1}$ $\mu_{2,1}$ and $\mu_{3,1}$ are all positive. This positiveness/negativeness property of $z_{k,1}$, $z_{k,2}$, $z_{k,3}$, and $z_{k,4}$ gives rise to the idea of the combining such four features in order to strengthen the detection accuracy of the input $s_k$. We elaborate our design of optimally-weighted combination strategy in the following.

### B. Optimally-Weighted Non-Coherent Detection

The key point of OWNCD is to derive optimal weights for the four extracted features, in order to minimize the BER. To do so, we express the weighted combination of the features, and the decision process leveraged on such a metric as:

$$z_k^{\text{OWNCD}} = w_1 \cdot z_{k,1} + w_2 \cdot z_{k,2} + w_3 \cdot z_{k,3} + w_4 \cdot z_{k,4} \underset{\hat{s}_k=0}{\overset{\hat{s}_k=1}{\gtrless}} \zeta, \tag{13}$$

where $w_1$, $w_2$, $w_3$, and $w_4$ are the corresponding weights, and $\zeta$ is the detection threshold. We next derive the optimal weights and the detection threshold by 1) analyzing the probabilistic distribution of the metric $z_k^{\text{OWNCD}}$, 2) computing the theoretical BER with respect to the optimal detection threshold

and different weights, and 3) computing the optimal weights $w_1$, $w_2$, $w_3$, and $w_4$ by minimizing the theoretical BER.

*1) Distribution of weighted combining metric:* With the help of Eq. (13) and the distributions of $z_{k,1}$, $z_{k,2}$, $z_{k,3}$, and $z_{k,4}$, the distribution of $z_k^{\text{OWNCD}}$ conditioned on $s_k$ is straightforward, i.e.,

$$z_k^{\text{OWNCD}}|s_k \sim \begin{cases} \mathcal{N}\left(\mu_0,\ \sigma^2\right) & s_k = 0, \\ \mathcal{N}\left(\mu_1,\ \sigma^2\right) & s_k = 0, \end{cases} \tag{14}$$

where $\mu_0$, $\mu_1$ is the the expectations under conditions of $s_k = 0$ and $s_k = 1$ respectively, and $\sigma^2$ is the variance, i.e., $\mu_0 = \sum_{d=1}^{4} w_d \cdot \mu_{d,0}$, $\mu_1 = \sum_{d=1}^{4} w_d \cdot \mu_{d,1}$ and $\sigma^2 = \sum_{d=1}^{4} w_d^2 \cdot \sigma_d^2$.

*2) Theoretical BER computation:* Given the Gaussian distribution of $z_k^{\text{OWNCD}}$ in Eq. (14), the theoretical BER of Eq. (13) can be computed as:

$$\begin{aligned} \text{BER} =& \Pr\{s_k = 0\} \cdot \Pr\{\hat{s}_k = 1 | s_k = 0\} \\ &+ \Pr\{s_k = 1\} \cdot \Pr\{\hat{s}_k = 0 | s_k = 1\} \\ =& \frac{1}{2\sqrt{2\pi}\sigma} \left( \int_{\zeta}^{+\infty} e^{-\frac{(z-\mu_0)^2}{2\sigma^2}} dz + \int_{-\infty}^{\zeta} e^{-\frac{(z-\mu_1)^2}{2\sigma^2}} dz \right) \end{aligned} \tag{15}$$

where $\Pr\{\cdot\}$ represents the probability of the event. Here, without loss of generality, we assume $\Pr\{s_k = 0\} = \Pr\{s_k = 1\} = 0.5$, corresponding to equal probabilities of the emitted symbols $s_k = 0$ and $s_k = 1$.

Accordingly, the optimal detection threshold that minimizes the BER in Eq. (15) is straightforward, being

$$\zeta = \frac{\mu_1 + \mu_0}{2}. \tag{16}$$

By taking Eq. (16) back into Eq. (15), the BER can be further deduced as a function of the weights $w_1$, $w_2$, $w_3$, and $w_4$, i.e.,

$$\begin{aligned} \text{BER}(w_1, w_2, w_3, w_4) =& Q\left( \sqrt{\frac{(\mu_1 - \mu_0)^2}{4\sigma^2}} \right) \\ =& Q\left( \sqrt{\frac{\left(\sum_{d=1}^{4} w_d(\mu_{d,1} - \mu_{d,0})\right)^2}{4\sum_{d=1}^{4} w_d^2 \sigma_d^2}} \right), \end{aligned} \tag{17}$$

where $Q(x) = \int_x^{+\infty} 1/\sqrt{2\pi} e^{-z^2/2} dz$. As such, given the relationship between BER and the weights in Eq. (17), we next compute the optimal weights by minimizing Eq. (17).

*3) Optimal weight computation:* We at first explain the existence of the minimum BER. This is due to the fact that values of SNR for the four metrics $z_{k,1}$, $z_{k,2}$, $z_{k,3}$, and $z_{k,4}$ are finite, and therefore the SNR of the linear combination of such metrics is inevitable bounded and there exists an upper-bound of SNR that is associated to the lowest BER.

Given the theoretical BER in Eq. (17), the computation of its minimum is to find the solution of $w_1$, $w_2$, $w_3$, and $w_4$ such that:

$$\frac{\partial \text{BER}(w_1, w_2, w_3, w_4)}{\partial w_n} = 0, \quad n = 1, 2, 3, 4. \tag{18}$$

We further simplify Eq. (18) by analyzing the SNR in the function of $Q(\sqrt{\text{SNR}})$ in Eq. (17), where $Q(x)$ is monotonically decreasing with the increment of $x$. As such, by expressing the SNR as:

$$\text{SNR}(w_1, w_2, w_3, w_4) = \frac{\left(\sum_{d=1}^{4} w_d(\mu_{d,1} - \mu_{d,0})\right)^2}{4\sum_{d=1}^{4} w_d^2 \sigma_d^2}, \tag{19}$$

solving Eq. (18) is converted to solving $\frac{\partial \text{SNR}}{\partial w_1} = \frac{\partial \text{SNR}}{\partial w_2} = \frac{\partial \text{SNR}}{\partial w_3} = \frac{\partial \text{SNR}}{\partial w_4} = 0$. By denoting $\varrho_d = \mu_{d,1} - \mu_{d,0}$ by $d = 1, 2, 3, 4$, the left hand side of this equation is further computed as:

$$\begin{aligned} \frac{\partial \text{SNR}}{\partial w_n} &= \frac{\varrho_n \sum_{d=1}^{4} w_d \varrho_d \sum_{d=1}^{4} w_d^2 \sigma_d^2 - w_n \sigma_n^2 \left(\sum_{d=1}^{4} w_d \varrho_d\right)^2}{2\left(\sum_{d=1}^{4} w_d^2 \sigma_d^2\right)^2} \\ &= \frac{\sum_{d=1}^{4} w_d \varrho_d}{2\left(\sum_{d=1}^{4} w_d^2 \sigma_d^2\right)^2} \left( \varrho_n \sum_{d=1}^{4} w_d^2 \sigma_d^2 - w_n \sigma_n^2 \sum_{d=1}^{4} w_d \varrho_d \right). \end{aligned} \tag{20}$$

Thus, it can be converted to:

$$\varrho_n \sum_{d=1}^{4} w_d^2 \sigma_d^2 - w_n \sigma_n^2 \sum_{d=1}^{4} w_d \varrho_d = 0. \tag{21}$$

Noticing from Eq. (21), we have:

$$\frac{w_1 \sigma_1^2}{\varrho_1} = \frac{w_2 \sigma_2^2}{\varrho_2} = \frac{w_3 \sigma_3^2}{\varrho_3} = \frac{w_4 \sigma_4^2}{\varrho_4} = \frac{\sum_{d=1}^{4} w_d^2 \sigma_d^2}{\sum_{d=1}^{4} w_d \varrho_d} = \xi, \tag{22}$$

which indicates the proportional relationship among $w_1$, $w_2$, $w_3$, and $w_4$. To be specific, by assigning $\xi$ as any positive (real) value, we can derive a group of weights to be:

$$w_d = \xi \cdot \frac{\mu_{d,1} - \mu_{d,0}}{\sigma_d^2}, \ d = 1, 2, 3, 4 \tag{23}$$

which ensures $\frac{\partial \text{SNR}}{\partial w_1} = \frac{\partial \text{SNR}}{\partial w_2} = \frac{\partial \text{SNR}}{\partial w_3} = \frac{\partial \text{SNR}}{\partial w_4} = 0$. Therefore, such derived $w_1$, $w_2$, $w_3$, and $w_4$ can guarantee a minimum BER. It is noteworthy that, the solutions are a series of values with any positive $\xi$, all of which give the same BER that is not related to $\xi$ in Eq. (24) by taking Eq. (23) into Eq. (17), i.e.,

$$\text{BER}_{\text{min}} = Q\left( \sqrt{\frac{\sum_{d=1}^{4} \frac{(\mu_{d,1} - \mu_{d,0})^2}{\sigma_d^2}}{4\sum_{d=1}^{4} (\mu_{d,1} - \mu_{d,0})^2}} \right). \tag{24}$$

Thus, the best BER performance will be obtained when the weights of the metrics are derived from Eq. (23).

Compared with previous non-coherent detection methods, OWNCD is able to achieve a better communication accuracy, attributed to the derivation of the optimal weights. However, such computation of the optimal weights requires partial channel information (i.e., the expectations and the variances of $z_{k,1}$, $z_{k,2}$, $z_{k,3}$, and $z_{k,4}$). To do so, traditional channel estimation technologies (e.g.the ML approach) require a large pilot sequence overhead (repeatedly for time-varying UVC channels), and extensive computational resources due to the computation of the exponential/logarithm -form of likelihood PDF, which make them unattractive. Instead, we design a heuristic algorithm to recursively compute such channel information, but avoid the complex channel estimation process.

### C. Heuristic algorithm

The heuristic algorithm is used to adaptively reach the optimal weights with the change of unknown CIR. For the first $k_0$ symbols, we assign $w_1 = w_2 = w_3 = w_4 = 1$ for metric combination, and the signal detection can be pursued by:

$$z_k = \sum_{d=1}^{4} z_{k,d} \underset{\hat{s}_k=0}{\overset{\hat{s}_k=1}{\gtrless}} \eta_k, \ \eta_k = \frac{1}{k}\sum_{k'=1}^{k} z_{k'} \tag{25}$$

Then, for $(k > k_0)$th symbol, we compute the expectations and variances (i.e., $\mu_{d,1}$, $\mu_{d,0}$, $\sigma_d^2$ with $d = 1, 2, 3, 4$) via the previous $k_0$ data, i.e.,

$$\mu_{d,0} = \frac{1}{|\mathcal{K}_0|}\sum_{k'\in\mathcal{K}_0} z_{k',d}, \quad d = 1, 2, 3, 4 \tag{26}$$

$$\mu_{d,1} = \frac{1}{|\mathcal{K}_1|}\sum_{k'\in\mathcal{K}_1} z_{k',d}, \quad d = 1, 2, 3, 4 \tag{27}$$

$$\sigma_d^2 = \frac{1}{k_0}\left(\sum_{k'\in\mathcal{K}_0}\left(z_{k',d} - \mu_{d,0}\right)^2 + \sum_{k'\in\mathcal{K}_1}\left(z_{k',d} - \mu_{d,1}\right)^2\right) \tag{28}$$

where $\mathcal{K}_0 = \{k' | \hat{s}_{k'} = 0, k - k_0 \le k' < k\}$, and $\mathcal{K}_1 = \{k' | \hat{s}_{k'} = 1, k - k_0 \le k' < k\}$, and we have $|\mathcal{K}_0| + |\mathcal{K}_1| = k_0$. Leveraged on Eqs. (26)-(28), the OWNCD metric $z_k^{\text{OWNCD}}$ in Eq. (13), and the decision threshold $\zeta$ in Eq. (16) can be computed, and the decision can be pursued.

As such, the heuristic algorithm avoids the usages of the pre-defined pilot sequence and the complex channel estimation process, rather it relies on only the basic adder and multiplier, which makes it easy for implementation and energy-saving.

## IV. Numerical Simulations

In the following analysis, the performance of our proposed OWNCD scheme is evaluated. Here, the detection accuracy is measured via the BER, and the computational complexity is approximated by the number of multiplications needed.

The parameters involved are configured in accordance with the study in [22], which is typical for a UVC scattering system using a UV-LED transmitter. The number of emitted photons for each '1'-bit is taken as $N_T = 1.7 \times 10^{13}$. The transmission distance is set at 250m. The transmitter's beam divergence and apex angle are $\pi/12$ and $\pi/4$, respectively. The receiver's half-field of view and apex angle are $\pi/12$ and $\pi/4$, respectively. The atmospheric coefficients are $\kappa_a = 5 \times 10^{-4} m^{-1}$ and $\kappa_s = 4.9 \times 10^{-4} m^{-1}$. For simulating different levels of ISI, we set the symbol rate in the range $R_b = 1/T_b \in [4 \times 10^6 \text{bit/s}, \ 5 \times 10^6 \text{bit/s}]$. Similarly, we consider SNR values from 5 dB and 25 dB in order to test the BER versus different intensities of ambient noise. Given the aforementioned channel parameters, different CIRs of the UV channel are generated via the Monte-carlo simulator [10], [11]. For both the previous non-coherent scheme in [30] and the proposed OWNCD, we assign a constant number of samples $M = 20$, evenly sampled for each symbol.

For comparison, we choose the non-coherent scheme for molecular communications in [30], and the state-of-the-art coherent MLSD for generic FSOs in [20], for the following two reasons. First, molecular communications and UVC share similarity, as both models are based on independent particle (e.g., molecules and UV photons respectively) motion. As such, we aim to show the necessity of the design of OWNCD, by testing whether the non-coherent scheme for molecular communications is suitable for UVC. Second, in most of the cases (including UVC), MLSD has been proved to have lowest BER when CSI is accurately derived, but consumes substantial computational and storage resources for CSI estimation and signal detection. In this view, we aim to demonstrate the communication performance of the proposed OWNCD for UVCs by comparing both BER and resource consumption.

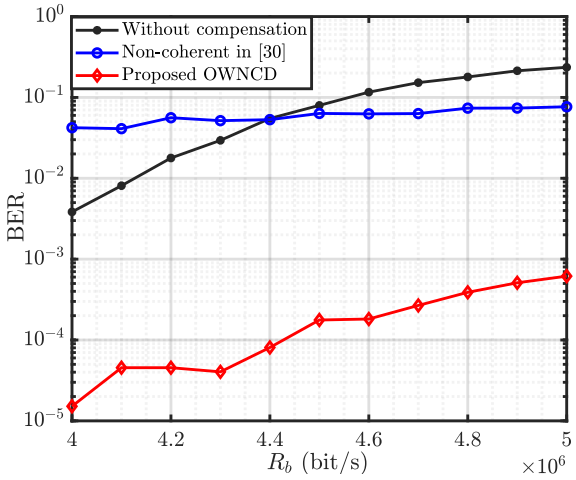


Fig. 3. BER versus different intensities of ISI (whose increase is reflected by the increase of symbol rate $R_b$). The slower growth of BER with the increase of the ISI indicate the abilities of the proposed OWNCD to combat ISI.

### A. BER versus ISI

We firstly evaluate the detection accuracy of the proposed scheme with respect to different levels of ISI intensity. For this investigation, we fix the SNR at 18 dB, and change the symbol rate $R_b$ that reflects different intensities of ISI.

It is observed that the proposed OWNCD improves the BER, by at least two orders of magnitude, compared to the direct detection and the previous non-coherent schemes in [30]. Such BER advantage over direct detection is attributed to the design of ISI-insensitive features, the combination of which enables a robust performance to ISI contamination. Then, when it comes to the comparison with previous non-coherent scheme in [30], the BER advantage comes from (i) the proposed OWNCD embraces the intra-symbol energy feature which is important for UVC, and has been ignored in [30]; (ii) the proposed OWNCD can derive the optimal weights, which indicates its ability to appropriately adjust the four metrics in accordance with the time-varying channel environment.

### B. Performance Comparison

We now compare the proposed OWNCD with the previous non-coherent scheme in [30], and with the state-of-the-art coherent MLSD in [20], in terms of both the BER and the computational complexity in Figs. 4-5. The first of these

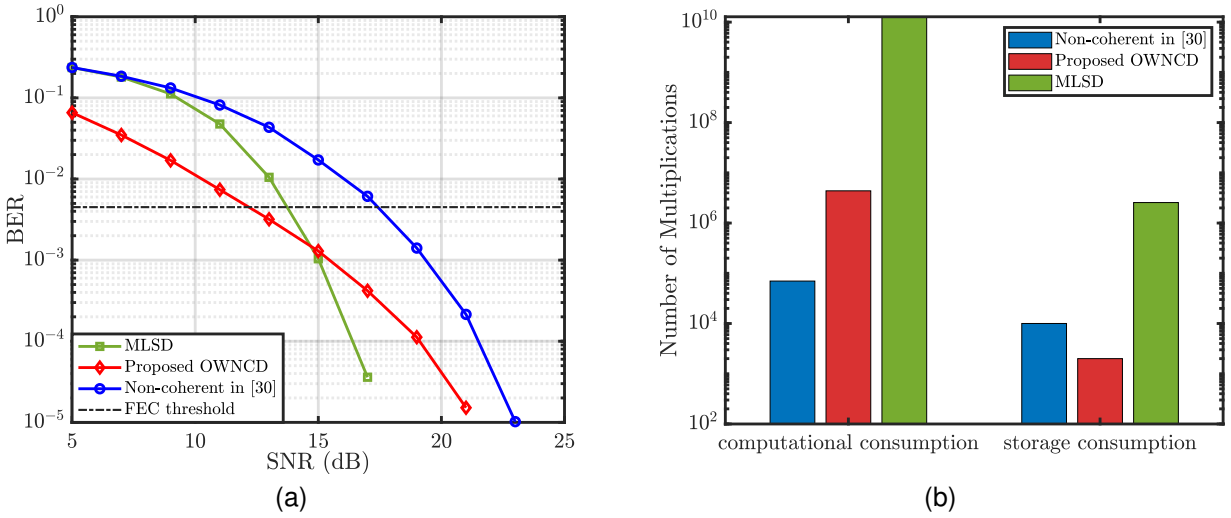


Fig. 4. Performance comparison between the proposed OWNCD, the previous non-coherent method in [30], and the state-of-the-art coherent MLSD [20] in a static channel: (a) BER comparison; (b) complexity comparison for $10^4$ bits.

studies the case with a static CIR, and the second considered performance comparison in the face of changing CIR.

*1) Comparison in static CIR:* It is seen from Fig. 4(a) that, the proposed OWNCD gains $\sim$ 4 dB in SNR compared to the non-coherent scheme in [30]. This is for the same reasons that the proposed scheme considers the intra-symbol neglected in [30] and more crucially assigns optimal weights to each features with respect to the specific ISI intensity rather equal weights as in [30].

Then, compared to the state-of-the-art MLSD, the proposed OWNCD provides a lower BER in small SNR region (i.e., SNR $<$ 15 dB), but higher BER when SNR is large. This is because the extracted features of the proposed OWNCD can combat ISI inherently. As such, it avoids channel estimation for ISI compensation which is vulnerable to the ambient noise (as the MLSD does). Then, when the SNR becomes large, the performance of the channel estimation becomes reliable, leading to the better performance of the MLSD.

However, it is noted that although the coherent MLSD shows a better performance in the high SNR region, the proposed OWNCD can reach the 7% overhead hard-decision FEC limit (BER = $4.5 \times 10^{-3}$) [31] faster (by more than 1 dB). This indicates that with a proper FEC code, the OWNCD can achieve an error-free transmission faster compared to the coherent MLSD. Moreover, when combining with the cost in Fig. 4(b), we can see that the proposed OWNCD has a great advantage in terms of both the computational complexity and storage resources. The proposed OWNCD has a complexity of the order of $10^6$, which is much less than that of the MLSD ($10^{10}$). Meanwhile, the storage consumption required for the proposed scheme is smaller compared with the coherent MLSD (around $10^4$ versus $10^6$).

Thus, our proposed OWNCD provides a low-complexity and low-storage based detection paradigm for the UVC scenarios, which can approach the detection accuracy of the coherent MLSD but with the benefit of lower computational resources.

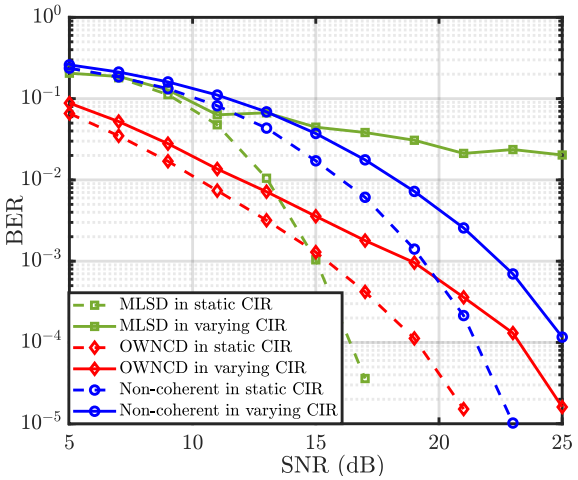


Fig. 5. BER comparison between the proposed OWNCD, the previous non-coherent scheme in [30], and the state-of-the-art coherent MLSD [20], in a time-varying channel.

*2) BER versus changing CIR:* A BER comparison with changing CIR is illustrated in Fig. 5. Here, the time-varying CIR is performed by adding process noise to the channel parameters, e.g., $r(k) = r(k-1) + \Delta_r$, and $\theta_R(k) = \theta_R(k-1) + \Delta_{\theta_R}$, indicating the slight disturbance given the flexible deployment of UVC.

In Fig. 5, we can firstly observe that the proposed OWNCD is robust in the case of the time-varying CIR, since its BER does not deteriorate drastically when compared with static CIR. This is mainly attributed to the heuristic algorithm, which updates the optimal weights and the threshold by the previous data that can reflect the continuous changes in the CIR. Meanwhile, we can observe that the coherent MLSD performs unreliably in dealing with the continuously varying channel ($>$8 dB loss in SNR is shown compared to the proposed OWNCD). This is because MLSD relies heavily on the estimated CIR from the pilot sequence, which may be

unreliable in the face of the time-varying channel environment, thereby resulting in unattractive detection accuracy.

As such, our proposed OWNCD are more suitable for counteracting the time-varying channel environment, which is closer to real UVC scenarios. Also, compared with the coherent schemes, the proposed OWNCD does not rely on complex channel estimation of the CIR, making them capable of saving computational and storage resources.

## V. Conclusion

For most sequential optical wireless detection scenarios, the signal detection without explicit channel information is challenging. Current bottlenecks lie in how to address the ISI from the long-tail and time-varying channel response. In this work, we have proposed a novel non-coherent paradigm by exploiting the inherent features, which are inherently insensitive to the ISI, of UV signals. Leveraged on the features, the optimally-weighted non-coherent detection (OWNCD) is developed, which enables the conversion of the signal detection with ISI into a binary detection framework. It is found that, compared to the state-of-the-art coherent MLSD, the proposed OWNCD scheme improves the detection accuracy by $\sim$1 dB for the static CSI and $\sim$8 dB for the time-varying CSI, in terms of SNR at the $7\%$ overhead FEC limit i.e., BER=$4.5 \times 10^{-3}$. In addition, it reduces the computational and storage resources by four order of magnitude. As such, our proposed feature-based non-coherent technique provides a promising pathway and novel insight for the efficient detection in complex and dynamic optical channels with intensive ISI.

## References


[1] A. Vavoulas, H. G. Sandalidis, N. D. Chatzidiamantis, Z. Xu, and G. K. Karagiannidis, "A survey on ultraviolet C-Band (UV-C) communications," *IEEE Commun. Surveys Tut.*, vol. 21, no. 3, pp. 2111–2133, thirdquarter 2019.

[2] M. A. El-Shimy and S. Hranilovic, "Binary-input non-line-of-sight solar-blind UV channels: Modeling, capacity and coding," *J. Opt. Commun. Netw.*, vol. 4, no. 12, pp. 1008–1017, Dec. 2012.

[3] D. Kedar and S. Arnon, "Subsea ultraviolet solar-blind broadband free-space optics communication," *Opt. Eng.*, vol. 48, no. 4, p. 046001, Apr. 2009.

[4] R. J. Drost and B. M. Sadler, "Survey of ultraviolet non-line-of-sight communications," *Semicond. Sci. Tech.*, vol. 29, no. 8, p. 084006, Jun. 2014.

[5] Z. Xu and B. M. Sadler, "Ultraviolet communications: potential and state-of-the-art," *IEEE Commun. Mag.*, vol. 46, no. 5, pp. 67–73, May 2008.

[6] G. A. Shaw, A. M. Siegel, and M. L. Nischan, "Demonstration system and applications for compact wireless ultraviolet communications," in *Sensors, and Command, Control, Communications, and Intelligence (C3I) Technologies for Homeland Defense and Law Enforcement II*, vol. 5071. International Society for Optics and Photonics, Sep. 2003, pp. 241–252.

[7] K.-X. Sun, B. Allard, S. Buchman, S. Williams, and R. L. Byer, "LED deep UV source for charge management of gravitational reference sensors," *Classical Quant. Gravity*, vol. 23, no. 8, p. S141, Mar. 2006.

[8] B. Albrecht, S. Kopta, O. John, M. Rütters, M. Kunzer, R. Driad, N. Marenco, K. Köhler, M. Walther, and O. Ambacher, "Improved AlGaN pin photodetectors for monitoring of ultraviolet radiation," *IEEE J. Sel. Topics Quantum Electron.*, vol. 20, no. 6, pp. 166–172, May 2014.

[9] H.-Y. Liu, W.-C. Hsu, B.-Y. Chou, and Y.-H. Wang, "Fabrication AlGaN/GaN MIS UV photodetector by H2O2 oxidation," *IEEE Photon. Technol. Lett.*, vol. 27, no. 1, pp. 101–104, Oct. 2014.

[10] H. Ding, G. Chen, A. K. Majumdar, B. M. Sadler, and Z. Xu, "Modeling of non-line-of-sight ultraviolet scattering channels for communication," *IEEE J. Sel. Area Commun.*, vol. 27, no. 9, pp. 1535–1544, Dec. 2009.

[11] R. J. Drost, T. J. Moore, and B. M. Sadler, "UV communications channel modeling incorporating multiple scattering interactions," *J. Opt. Soc. Am. A.*, vol. 28, no. 4, pp. 686–695, Apr. 2011.

[12] M. R. Luettgen, J. H. Shapiro, and D. M. Reilly, "Non-line-of-sight single-scatter propagation model," *J. Opt. Soc. Am. A.*, vol. 8, no. 12, pp. 1964–1972, Dec. 1991.

[13] R. J. Drost, T. J. Moore, and B. M. Sadler, "Ultraviolet scattering propagation modeling: analysis of path loss versus range," *J. Opt. Soc. Am. A.*, vol. 30, no. 11, pp. 2259–2265, Nov. 2013.

[14] M. A. Elshimy and S. Hranilovic, "Impact of finite receiver-aperture size in a non-line-of-sight single-scatter propagation model," *J. Opt. Soc. Am. A.*, vol. 28, no. 12, pp. 2568–2576, Dec. 2011.

[15] M. Wu, D. Han, X. Zhang, F. Zhang, M. Zhang, and G. Yue, "Experimental research and comparison of LDPC and RS channel coding in ultraviolet communication systems," *Opt. Express*, vol. 22, no. 5, pp. 5422–5430, Mar 2014.

[16] H. Qin, Y. Zuo, F. Li, R. Cong, L. Meng, and J. Wu, "Analytical link bandwidth model based square array reception for non-line-of-sight ultraviolet communication," *Opt. Express*, vol. 25, no. 19, pp. 22 693–22 703, Sep. 2017.

[17] W. Hu, M. Zhang, D. Han, Q. Chen, L. Ai, Q. Li, and Z. Ghassemlooy, "Research on channel-related polar code with an optimum code length for wireless ultraviolet communications," *Opt. Express*, vol. 25, no. 23, pp. 28 630–28 642, Nov. 2017.

[18] X. Liang, M. Zhang, X. Li, L. Ai, and Z. Ghassemlooy, "Security performance of LDPC and polar codes in UV wireless communications," in *in Proc. 1st West Asian Colloquium Opt. Wireless Commun., Isfahan, Iran*, Apr. 2018, pp. 1–6.

[19] N. D. Chatzidiamantis, G. K. Karagiannidis, and M. Uysal, "Generalized maximum-likelihood sequence detection for photon-counting free space optical systems," *IEEE Trans. Commun.*, vol. 58, no. 12, pp. 3381–3385, Dec. 2010.

[20] C. Gong and Z. Xu, "Channel estimation and signal detection for optical wireless scattering communication with inter-symbol interference," *IEEE Trans. Wireless Commun.*, vol. 14, no. 10, pp. 5326–5337, Oct. 2015.

[21] Z. Wei, W. Hu, M. Zhang, D. Han, B. Li, and C. Zhao, "Viterbi estimation on the finite-state markov ultra-violet channels," in *Asia Communications and Photonics Conference (ACP)*, Nov. 2017, pp. 1–3.

[22] Z. Wei, W. Hu, D. Han, M. Zhang, B. Li, and C. Zhao, "Simultaneous channel estimation and signal detection in wireless ultraviolet communications combating inter-symbol-interference," *Opt. Express*, vol. 26, no. 3, pp. 3260–3270, Feb. 2018.

[23] D. Zou, C. Gong, and Z. Xu, "Signal detection under short-interval sampling of continuous waveforms for optical wireless scattering communication," *IEEE Trans. Wireless Commun.*, vol. 17, no. 5, pp. 3431–3443, May 2018.

[24] X. Dai, S. J. Sheard, D. O'Brien, S. Russell, and L. Carswell, "Propagation and scattering model of infrared and ultraviolet light in turbid water," in *2013 22nd Wireless and Optical Communication Conference*, 2013, pp. 601–606.

[25] D. Moriarty and B. Hombs, "System design of tactical communications with solar blind ultraviolet non line-of-sight systems," in *MILCOM 2009 - 2009 IEEE Military Communications Conference*, 2009, pp. 1–7.

[26] Z. Wei, W. Guo, B. Li, J. Charmet, and C. Zhao, "High-dimensional metric combining for non-coherent molecular signal detection," *IEEE Transactions on Communications*, vol. 68, no. 3, pp. 1479–1493, Mar. 2020.

[27] X. Zhu and J. M. Kahn, "Free-space optical communication through atmospheric turbulence channels," *IEEE Trans. Commun.*, vol. 50, no. 8, pp. 1293–1300, Nov. 2002.

[28] J. Li, J. Q. Liu, and D. P. Taylor, "Optical communication using subcarrier PSK intensity modulation through atmospheric turbulence channels," *IEEE Trans. Commun.*, vol. 55, no. 8, pp. 1598–1606, Aug. 2007.

[29] M. L. B. Riediger, R. Schober, and L. Lampe, "Multiple-symbol detection for photon-counting MIMO free-space optical communications," *IEEE Trans. Wireless Commun.*, vol. 7, no. 12, pp. 5369–5379, Dec. 2008.

[30] B. Li, C. Zhao, and W. Guo, "Non-linear signal detection for molecular communications," in *2017 IEEE Global Communications Conference*, Dec. 2017, pp. 1–6.

[31] F. Chang, K. Onohara, and T. Mizuochi, "Forward error correction for 100G transport networks," *IEEE Commun. Mag.*, vol. 48, no. 3, pp. S48–S55, Mar. 2010.